Supplementary Information

Use of Isotope-Edited FTIR to Derive a Backbone Structure of a Transmembrane Protein

Joshua Manor,[†] Eyal Arbely,[†,§] Andrè Beerlink,[‡,‖] Mutaz Akkawi,[¶] and Isaiah T. Arkin[*,†]

Department of Biological Chemistry, The Alexander Silberman Institute of Life Sciences, The Hebrew University of Jerusalem, Edmund J. Safra Campus, Jerusalem, 91904 Israel, Institut für Röntgenphysik, Georg-August-Universität Göttingen, Friedrich-Hund-Platz 1, Göttingen, 37077 Germany, and Faculty of Science & Technology Al-Quds University, Abu Dis.

E-mail: arkin@huji.ac.il

Supplementary background

SARS coronavirus

In the winter of 2002, a new devastating human disease, termed "severe acute respiratory syndrome" (SARS) emerged from the Far East.[1] Starting at November 2002, 8,422 SARS-related cases and 916 SARS-related deaths have been reported in 25 countries world-wide. Death from

[*]To whom correspondence should be addressed
[†]Jerusalem
[‡]Göttingen
[¶]Al-Quds
[§]Current address: Department of Chemistry, Ben-Gurion University of the Negev, Beer-Sheva, 84105, Israel
[‖]Current address: incoatec GmbH, Max-Planck-Strasse 2 Geesthacht, 21502, Germany

progressive respiratory failure occurred in just over 10% of cases, and peaked to almost 50% among elderly patients.[2]

The causative agent of SARS was quickly recognized as a coronavirus,[3] and its genome sequence indicated that it is new member of the Coronaviridae.[4,5] Even after the dwindling of the SARS pandemic in July 2003, new members of coronaviridae continue to be isolated from patients exhibiting respiratory diseases: By 2005 two new members were isolated in the Netherlands (HCoV-NL63)[6] and Hong Kong (HCoV-HKU1).[7] Late in 2012, MERS-CoV was isolated in Saudi Arabia,[8] as the causative agent of the "Middle East SARS" with a fatality rate close to 50%.

SARS coronavirus E protein

SARS-CoV has three membrane proteins:[1] (i) The trimeric fusion S(pike) glycoprotein that is functionally analogous to influenza's Hemagglutinin; (ii) The abundant polytopic M(embrane) glycoprotein, which gives the envelope its shape and (iii) The E(nvelope) small peptide, which is the subject of this study.

Found in small amounts in the virion's envelope, SARS-CoV's Envelope protein (E) is a small integral membrane protein composed of 76 amino acids.[9] Sequence comparison indicated that SCoV-E protein does not present significant homology to any other protein. Moreover, SCoV-E protein is also more conserved than other coronaviruses' E protein.[10] It lacks a signal peptide and does not undergo glycosylation.[1,11] However, palmitoylation on a conserved cysteine at the carboxy side of the transmembrane domain (TMD) does take place, and is essential for producing healthy viral particles.[12]

SCoV-E protein contains a TMD positioned near the N terminus, followed a long hydrophilic C terminus tail.[13,14] Its cytoplasmic tail is linked to an array of activities: It is sufficient to redirect the protein to the Golgi region;[15] It binds PALS1 tight junction protein, therefore potentially affecting cell polarity;[16] It contains a BH3-like region that interacts with Bcl-xL antiapoptotic protein, thus promoting apoptosis in T cells;[17] and also Down-regulates inositol-requiring enzyme 1 pro apoptotic pathway thus reducing apoptosis in other cells.[18]

The TMD of SCoV-E protein was found to form an ion channel, blocked by hexamethylene amiloride.[19] When the TDM, flanked by two lysine residues, was reconstituted in lipid bilayers it formed a Na^+ channel that could be inhibited by amantadine.[20] Measurements of channel conductance for the putative channel were also performed in diphytanoyl phosphocholine lipids.[21] Expression of the SARS-CoV E protein in mammalian cells altered the membrane permeability of these cells,[22] as well as in *Escherichia coli.*[23] Finally, cation selective channel activity was recorded for E proteins from other coronaviruses such as: Human-22E9, mouse hepatitis virus (MHV) and infectious bronchitis virus (IBV) when placed in bilayers.[24,25]

Coronavirus E proteins have been implicated to play a central role in the virus budding and maturation process. Following translation, S, M and E proteins are inserted into the ER, from which they mature to the ER-Golgi intermediate compartment.[1,26] The creation of new viral particles requires both M and E proteins.[27–29] Very little is known about the process: The TMD of E in IBV was found to alter the trafficking of cargos in infected cells to the advantage of the virus.[30] E and S structural proteins were found to decrease the levels of ENaC Na^+ channels at the apical surfaces of lung epithelial cells, possibly by activating the PKC pathway.[31] Expressing E alone resulted in the budding of vesicles containing E,[32] while complete deletion of E resulted in the budding of plaques with low growth rate and low infectious titer.[33–35] Expression of MHV-CoV E protein induced membrane curvature[36] and similarly, SCoV-E protein TMD incorporated in 1,2-dimyristoyl-sn-glycero-3-phosphocholine (DMPC) vesicles induced a significant degree of deformity to the vesicles.[13] E turnover seems to be governed by both the ubiquitination pathway employing nsp3[37] and ubiquitin-independent pathway by 8b.[38,39]

Recently, vaccination with SARS-CoV lacking E completely protected mice from lethal disease.[40] Not only the lack of E but also the presence of E can account for immunization targets, whereby individuals recovering from SARS showed marked T cell response when stimulated with peptides overlapping E sequence.[41] Also, snRNAs targeting the gene of E delivered in adenovirus vector significantly inhibited the expression of SARS-CoV genes in infected cell lines.[42,43] Deletion of E however still elicited a T and B cell immune response in susceptible mice[44] and ham-

sters.[35,45]

Topology analyses using immunofluorescence of epitope-tagged SCoV-E protein revealed that both termini of the protein are exposed to the cytoplasmic side of the membrane,[46] consistent with the finding on MHV's E,[47] but in contrast to IBV's E.[46] Moreover, X-ray reflectivity studies revealed that a phenylalanine residue located in the middle of TMD of the protein was positioned close to the lipid head group of DMPC bilayers.[48] E peptide did not change structurally under FTIR investigation when treated with protease K (data not shown) consistent with previous results demonstrating that MHV-CoV E was not affected by protease digestion.[36]

Spanning 28 amino acids, the TMD of SCoV-E protein is abnormally long[13] in comparison to the average TMD helix length of 21 residues.[49] Nevertheless, the TMD was shown by FTIR studies to be highly helical.[10,13,50] Finally, SCoV-E protein TMD was found to be pentameric[19] similar to the full length protein when expressed in *Escherichia coli*.[14]

Supplementary Material and Methods

Sample preparation

Peptide synthesis The peptide sequence used in all experiments encompassed the entire hydrophobic domain of SCoV-E protein (accession number NP_828854), and corresponded to residues E7-R38, as shown in Figure S1a. The peptides were synthesized using standard solid-phase N-(9-fluorenyl) methoxycarbonyl chemistry. A total of 19 hydrophobic residues along the peptide sequence were individually labeled using the $^{13}C{=}^{18}O$ double label at the positions indicated in red in Figure S1a. The $^{13}C{=}^{18}O$ double label was synthesized from 1-^{13}C labeled amino acids precursors (Cambridge Isotopes Laboratories, Andover, MA) according to previously published procedures.[51] In addition, three peptides, each containing a single *para*-iodo-phenylalanine, were synthesized using the same procedures. The location of the iodine labels is shown with a black asterisk in Figure S4.

Peptide purification The purification, and membrane reconstitution of the peptides used in this work have been described elsewhere.[13] In brief, ca. 2 mg of synthesized peptide were dissolved in 2 ml of trifluoroacetic acid, and injected into a 1×25 cm Jupiter 5 C4-300 Å column (Phenomex, Cheshire, UK) equilibrated with 80% H_2O, 8% (v/v) acetonitrile and 12% (v/v) isopropanol. Peptide elution was obtained with a linear gradient to a final solvent composition of 40% acetonitrile and 60% isopropanol. All solvents contained 0.1% (v/v) trifluoroacetic acid. Chromatography fractions containing the peptide were subsequently lyophilized.

Peptide reconstitution The peptides were reconstituted into lipid vesicles of 1,2-dimyristoyl-sn-glycero-3-phosphocholine (DMPC, Avanti polar lipids, Alabaster, Al) by co-solubilization in 1,1,1,3,3,3-hexafluoro-2-propanol (Merck, Whitehouse Station, NJ). Following rotoevaporation and desiccation, liposomes were prepared by hydration of the sample in 1 ml of water. Reconstituted liposomes were routinely sonicated using a probe-type sonicator for 2 minutes at 100 Watt (pulses given every 2 seconds) and extruded through 0.2 μm nitrocellulose filter at 37°.

FTIR spectroscopy

Spectra collection 400 μl of sample were deposited onto a 25 reflection Germanium internal reflection element ($2 \times 20 \times 50$ mm, Grasbey Specac, Kent, UK), followed by bulk solvent removal under a stream of dry, CO_2-depleted air for several hours. For each spectrum, 1000 interferograms at a resolution of 2 cm^{-1} were collected and averaged. Spectra were processed with 1-point zero filling and Happ-Genzel apodization. Polarized spectra were obtained with a 0.25 mm wire grid polarizer (Graseby Specac, Kent, UK). Two to four spectra were taken for each of the 19 different $^{13}C{=}^{18}O$ double-labeled peptides.

Peak fitting and integration In order to obtain orientational information from FTIR, peak integration and consequently peak fitting are required. Two peak fitting procedures were employed to reach a self-consistent result: (i) Peaks in the region between 1520 cm^{-1} and 1800 cm^{-1} were

approximated by corresponding Voigt functions and integrated separately. The baseline was taken as a linear line calibrated by the featureless area between 1900 cm^{-1} and 2500 cm^{-1}. (ii) Alternatively, the site-specific peaks were approximated as individual peaks as described in.[52] Finally, in both fitting procedures, the Gaussian full width at half height (FWHH) was estimated from the total Voigt FWHH and Lorentz FWHH and was averaged for all fitting procedures. Errors in the Gauss FWHH estimations are $\leq 0.02\%$, which is significantly lower than the discrepancy between the two peak fitting methods.

Orientational analyses

After FTIR spectra acquisition, the tilt angle between the amide I transition dipole moment (TDM) and the z axis was extracted as described in detail in.[53] In brief, the dichroic ratio $\mathscr{R}$, which is the ratio of absorption between parallel and perpendicular polarized light in attenuated total internal reflection (ATR) geometry is given by:

$$\mathscr{R}^{ATR} = \frac{\mathscr{E}_z^2 \, \mathscr{K}_z + \mathscr{E}_x^2 \, \mathscr{K}_x}{\mathscr{E}_y^2 \, \mathscr{K}_y}. \tag{1}$$

$\mathscr{E}_{x,y,z}$ are the axial electric field components given by Harrick[54] and $\mathscr{K}_{x,y,z}$ are the corresponding integrated, dimensionless, absorption coefficients for each of the three axes. In a uniaxial symmetric system, such as a lipid bilayer, the integrated absorption coefficients are given by:

$$\mathscr{K}z = \cos^2\theta \text{ and } \mathscr{K}x = \mathscr{K}y = \frac{1}{2}\sin^2\theta, \tag{2}$$

where θ is the angle between the vibration's TDM and the laboratory z axis. Since the lipid bilayer resides in the xy plane, the z axis is simply the bilayer normal. Note that the above is correct only when sample mosaicity is negligible,[55] which can easily be confirmed using X-ray reflectivity, as elaborated below.

The sample thickness significantly exceeds the penetration depth of the evanescent wave, allowing us to employ the thick film approximation.[56] Therefore, using refractive indices for Ge and

for the lipid bilayer of 4 and 1.43, respectively, we obtain: $\mathscr{E}_x = 1.398$, $\mathscr{E}_y = 1.516$ and $\mathscr{E}_z = 1.625$. Finally, incorporating the above parameters in equations Eq. (1) and Eq. (2), one obtains the tilt angle of the TDM from the z axis as a function of the measured dichroic ratio using the following simple relationship:[53]

$$\theta = \arctan\sqrt{\frac{2.14153}{\mathscr{R}^{ATR} - 0.923832}} \tag{3}$$

X-ray reflectivity

Mosaicity measurement Mosaicity of the membrane due to the incorporation of the peptide was measured using X-ray reflectivity rocking scans, as described in detail in.[55] Briefly, after a scattering profile is obtained, the angles of the incident and reflected beams were set to match the first Bragg peak. Subsequently, a rocking scan was conducted by tilting the sample perpendicularly to the X-ray beam. The change in intensity as a function of the rocking angle is then fit to a Gaussian profile, to derive the standard deviation σ, of the mosaicity. When the standard deviation is smaller than 5°, the mosaicity of the sample may be neglected and the orientational information can be extracted directly from the linear dichroism results using equation Eq. (3).[55]

Electron density profile construction Three samples were analyzed for electron density, each containing a single para-iodo-phenylalanine instead of phenylalanine in either one of the three naturally appearing in the peptide: F20, F23 and F26 (see Figure S4). In brief, samples were dissolved in chloroform/2-propanol (40:60% v/v) at 2 mg/ml, while DMPC lipids were dissolved in 20 mg/ml of chloroform/2-propanol (50:50% v/v). Stocks were mixed together to prepare samples at 1:10 or 1:50 protein:lipid molar ratio. Samples were then dried in water-deprived air and placed in a vacuum overnight, to remove traces of solvents. Following rehydration a film with a thicknesses of about 2-5 μm was obtained.

Electron density profiles were obtained by the Fourier synthesis method from the integrated peak intensities, using a Lorentz correction factor of $1/q_z$, and the following phases (+, -, -, - and -). The integrated intensity of the first Bragg peak was normalized to 1 for the non-iodinated SCoV-

E peptide, while the iodinated SCoV-E protein curves were properly scaled to the non-iodinated curve corresponding to the respective scattering signals.

Structural modeling

Two approaches for structural modeling of the SCoV-E protein based on orientational restraints were used: rigid body modeling and flexible molecular dynamics (MD) based refinement. In both approaches the aim was to derive a model, in which the differences between the experimental tilt angles and those found in the model are the smallest, while keeping with correct protein geometry.

Error calculation

Since the absorption of light is proportional to the squared scalar product of the electric field vector and the integrated absorption coefficient, angular ambiguity arises. In other words, while the calculated angle from the dichroism experiment is invariably in the first quadrant ($0 \leq \theta \leq \pi/2$), the actual angle might be any of the following four equal options: θ, $-\theta$, $\pi+\theta$ or $\pi-\theta$. Therefore, the difference Δ, between the experimental tilts θ, and the tilt angles for any model obtained ϑ, was calculated as the minimum of the following four options:

$$\Delta = min\{|\vartheta-\theta|, |\vartheta+\theta|, |\vartheta-(\pi-\theta)|, |\vartheta-(\pi+\theta)|\} \tag{4}$$

Rigid body refinement

Rigid body refinement was carried out as described elsewhere.[57] An ideal α-helix corresponding to the sequence of SCoV-E protein was constructed using PyMOL (Schrödinger, NY). The peptide was initially oriented such that its director coincided with the z axis. Afterwards, the peptide was tilted by 1° increments until complete inversion took place. At each tilt angle the peptide was rotated about its long axis (1° increments) until a complete revolution was obtained. For each rotation and tilt angle combination the amide I TDM tilt angles of the labeled residues were extracted and compared to the angles obtained experimentally. The difference between the experimental

results and those measured from the model reflected how well a particular structure abides by the experimental constraints.

MD based refinement

The procedure for using MD based refinement to yield structures of membrane proteins was recently detailed in.[53] Below we describe the basic principles of the procedure:

Set up MD simulations were carried out using CNS,[58,59] employing an annealing protocol for both the temperature and the Van der Waals force constant. The peptide was constructed as an ideal helix using PyMOL and included two dummy atoms to represent every one of the 19 labeled sites. The exact geometry of the atoms within the peptide group plane, was such that the angle between the two dummy atoms coincided exactly with the TDM of the amide I vibrational mode (see green atoms in Figure 3a). The two dummy atoms were constrained to their position using bond, angle and dihedral terms. However, they did not participate in any non-bonded interactions. All other force field parameters employed default values using the OPLS parameter set with a united atom topology.[60]

Experimental refinement At each MD simulation step the angle between the vector connecting the two dummy atoms and the z axis was calculated (ϑ). Subsequently the angle was restrained to the FTIR measured angle (θ) for the corresponding residue according to the following energy penalty function:

$$E = k\Delta^2, \tag{5}$$

where k is the harmonic force content equal to 400 kcal/(rad^2·mol), and Δ is the difference between the experiments results and that measured currently as detailed above.

As indicated, different segments of the protein were restrained to a helical geometry by an NOE restraint between the carbonyl oxygen of residue i and the amide proton of residue $i+4$. The NOE distance was set to 3.15 Å with a force constant of 200 kcal/(Å^2·mol). In the regions that

were restrained to a helical geometry, the orientational refinement was calculated as follows: The differences between the current angle ϑ, and the experimentally derived angle θ, was the minimum of the following two terms:

$$\Delta = min\{|\vartheta - \theta|, |\vartheta + \theta|\}, \tag{6}$$

whenever the helix that is tilted from the z axis by an angle smaller than $\pi/2$. When the helix tilt angle was larger than $\pi/2$, the difference between the current tilt angles and the experimental results were taken as the minimum of:

$$\Delta = min\{|\vartheta - (\pi - \theta)|, |\vartheta - (\pi + \theta)|\}. \tag{7}$$

See Figure 3b for a scheme of the two different calculation options in a case of a helical geometry. When the region was not restrained to an α-helical geometry, all four quadrants were used to calculate the difference from the experiential data (as implemented in equation Eq. (4)).

Annealing protocol Numerous protocols were tested in order to reach a consistent answer that yields the smallest difference from the experimental data (*i.e.* maximal refinement) while maintaining correct geometry. The temperature in the simulations was reduced linearly from 598°K to 273°K in 15°K increments (22 cycles), while the Van der Waals force was multiplied by an exponentially increasing constant from 0.03 to 1 in each cycle. The number of simulation steps in each cycle was determined by the total simulation length. Simulation steps were 0.1 fs and the total length of the simulation was 20 ps, after which additional convergence was not obtained.

Disulfide cross linking

Two peptides were synthesized, each with a pair of mutations: S16C and T35C in the first peptide and S16C and T30C and in the second (see Figure 2). In both samples A22 was labeled with a $^{13}C{=}^{18}O$. Reconstituted and hydrated (2 ml) samples were split into two identical aliquots of 1 ml each, alongside 100 μl of 150 mM Cu(II)(1,10-Phenanthroline)3, as an oxidation catalyst. The

aliquots were incubated at 37°C for 45 min. To one of the aliquots, 410 μl of 0.1 M Ethylenediaminetetraacetic acid (pH 8) were added at the end of the 45 min reaction, thereby chelating Cu(II) and terminating the oxidation reaction. In contrast, in the control aliquot, Ethylenediaminetetraacetic acid was added at the beginning of the incubation, thereby preventing oxidation from to taking place in the first place.

Subsequently, 2 ml of 1,1,1,3,3,3-hexafluoro-2-propanol (Merck, Whitehouse Station, NJ) were added to dissolve the liposomes completely. 800 μL of Reaction Buffer solution, containing 0.1 M disodium phosphate buffer (pH 8) and 1 mM of Ethylenediaminetetraacetic acid, were added to each aliquot. The pH was maintained above 8 by adding 5 μL of 10 mM NaOH to the final solution and was checked by blotting a small amount on a pH paper.

Finally, 900 μl of each aliquot (either undergoing the redox reaction or the control) was taken and incubated for 30 min with increasing amounts of 25 mM Ellman's reagent (98%, Sigma-Aldrich, St. Louis, MO). The amounts of Ellman's reagent that were added were: 5 μl, 7.5 μl, 10 μl, 15 μl, 20 μl, 50 μl and 100 μl. The ratio between the final concentration of the Reaction Buffer and the Ellman's reagent was kept above 10:1 by adding additional 200 μl of Reaction Buffer when 20 μl or more of the reagent solution were added. When adding 100 μl of reagent, the ratio was not kept above 1:10 but was 5:1, in order to maintain a homogenous solution.

Solutions in glass cuvettes were taken to a spectrophotometer (Ultraspec 2100 pro, GE Healthcare, Piscataway, NJ) to measure absorption at 412 nm, which is indicative of free thiol groups. Absorption values were compared between the aliquot that underwent the oxidation reaction (Ethylenediaminetetraacetic acid was added at the end of the incubation) and the identical aliquot that did not undergo the redox reaction (Ethylenediaminetetraacetic acid was added at the beginning). Therefore, decreased absorption at 412 nm in the reaction relative to the control vial indicates that the oxidation took place.

Supplementary figures

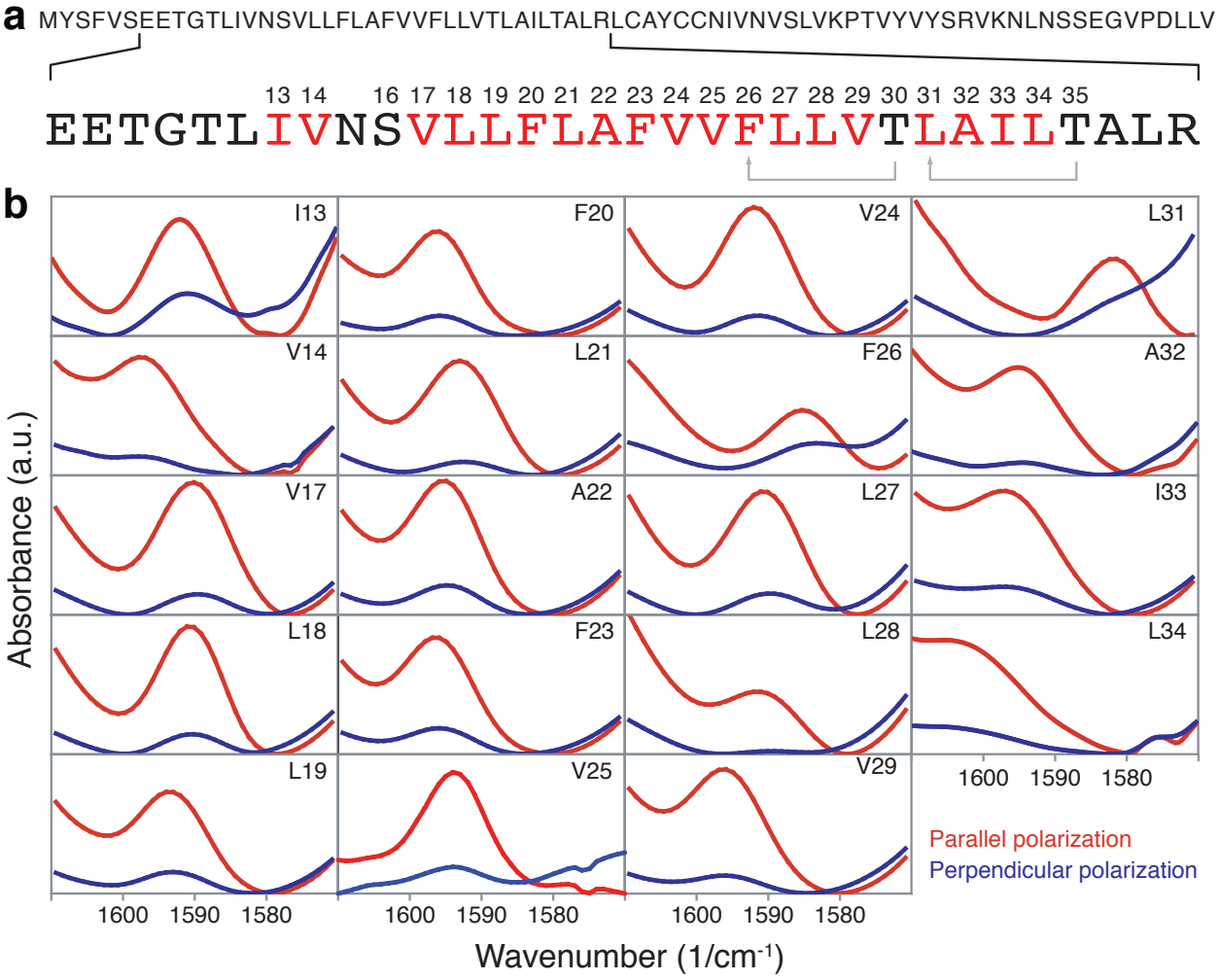

Figure S1. Sequence, labeling and FTIR spectra of the SCoV-E protein. a. Sequence of the SCoV-E protein (accession number NP_828854). The expanded region, E7-R38, indicates the transmembrane encompassing peptide that was used in all the experiments with red residues indicating positions of $^{13}C=^{18}O$ labeling. b. FTIR spectra in the region of the isotope-edited amide I mode of the different labeled peptides in hydrated lipid bilayers. Spectra were obtained using parallel (red) or perpendicular (blue) polarized light.

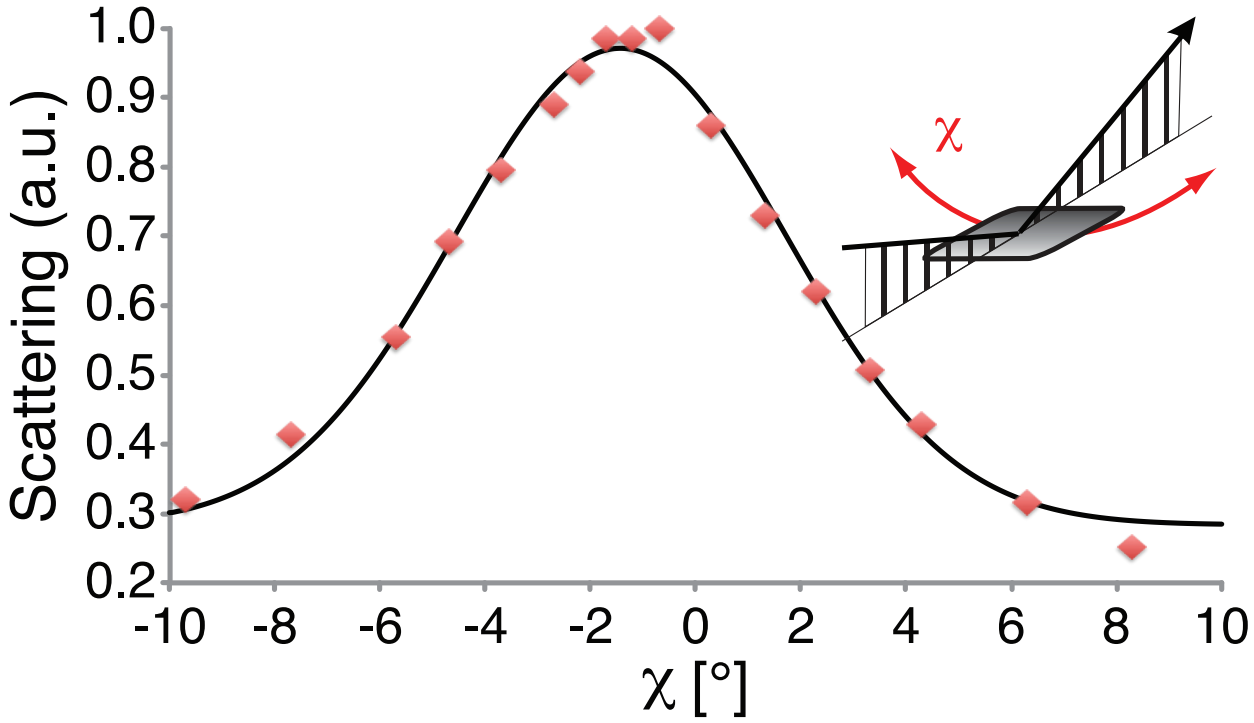

Figure S2. Membrane mosaicity measurement using X-ray reflectivity. Example χ scan on the first Bragg peak from a specular scan of the multi-lamellar SCoV-E protein lipid vesicles used for the FTIR analysis. See inset for a sketch of the experiment. The data (in red) are fit with a Gaussian function (solid line) with a standard deviation of $\sigma = 4.5°$, and are a measure of the probability distribution of local membrane normal vectors.

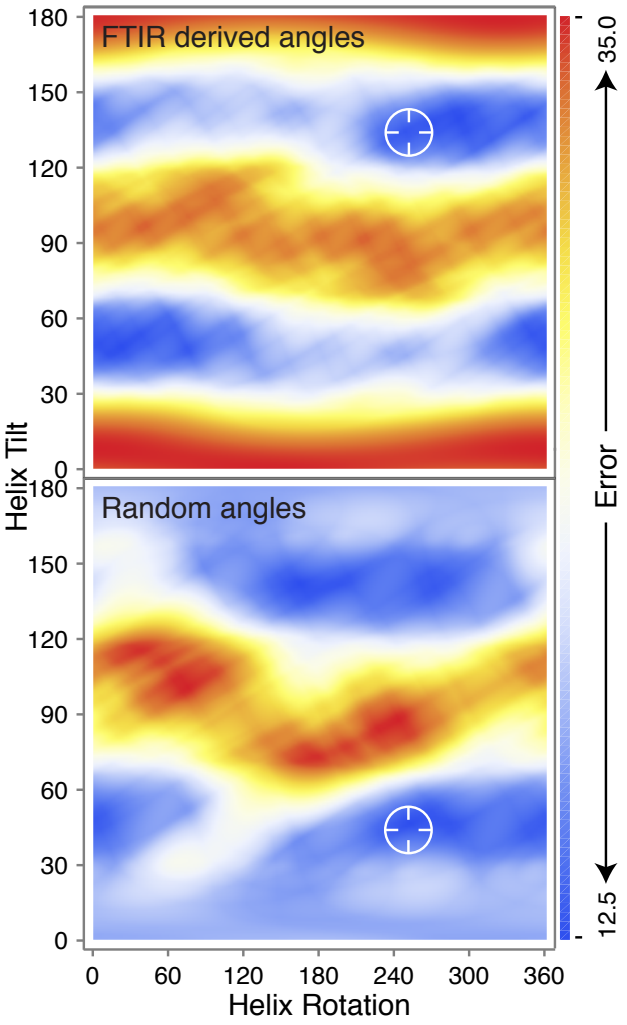

Figure S3. Rigid body modeling of the SCoV-E protein transmembrane domain. Each point in the graph represents a particular combination of tilt and rotation angles of an ideal helix. The color scale represents the TDM tilt angle difference per residue that the structure has relative to the angles derived from the FTIR study, or random angles in the top and bottom panels, respectively. The crosshair represents the minimum difference between the experimental data and the rigid body rotation.

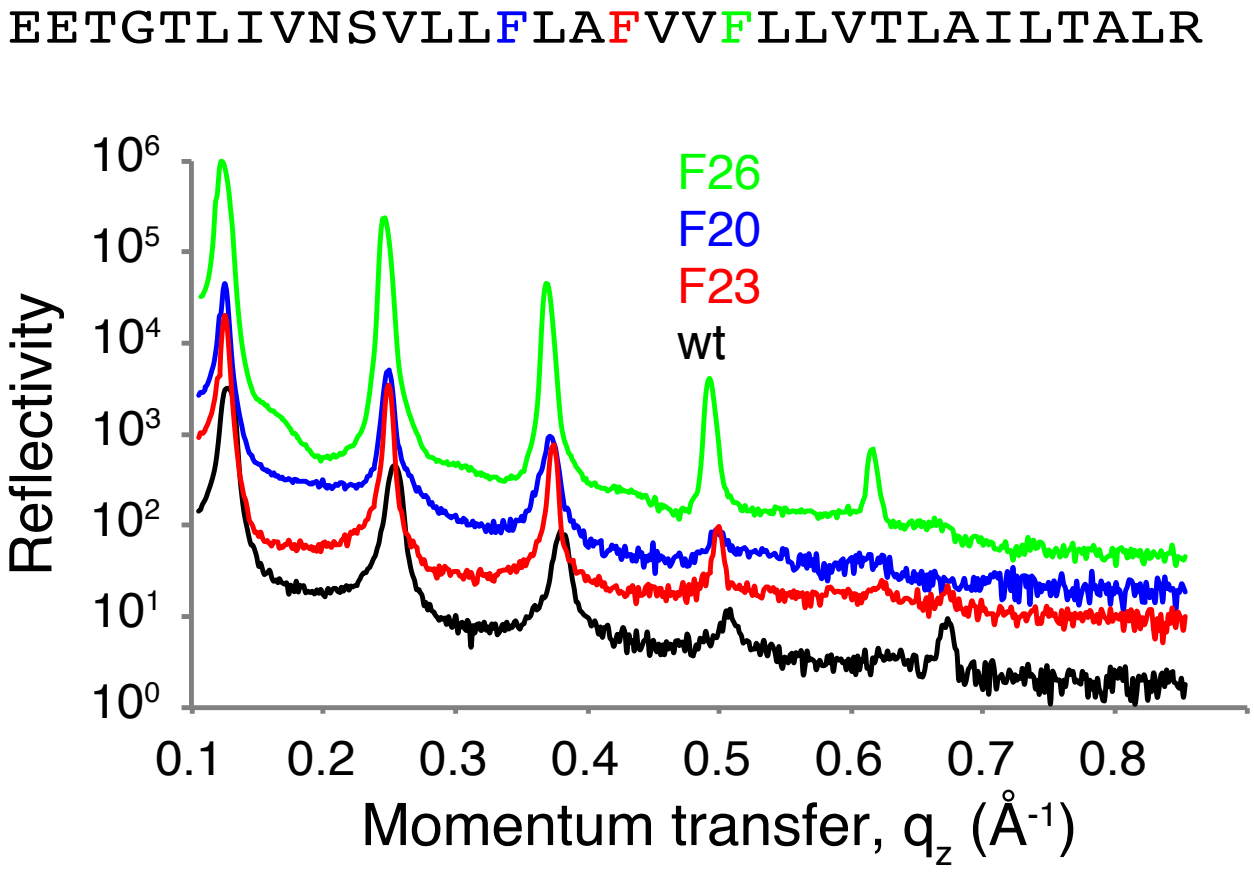

Figure S4. X-ray reflectivity of the SCoV-E protein in lipid bilayers. The sequence of the peptide indicating the positions of the different *para*-iodo-phenylalanine in color is shown at the top. bottom: Reflectivity curves of SCoV-E protein in hydrated multilamellar lipid bilayers. The wild type protein is in black, while the three para-iodinated phenylalanines containing peptides at residues F20, F23 and F26 are in blue, red and green, respectively. The curves are shifted vertically for clarity.

References

(1) Fields, B. N.; Knipe, D. M.; Howley, P. M. *Fields virology*, 6th ed.; Wolters Kluwer / Lippincott Williams & Wilkins Health: Philadelphia, 2013.

(2) WHO, World health organization summary table of sars cases by country 1 November 2002 - 7 August 2003 **2003**, *78*.

(3) Ksiazek, T. G.; Erdman, D.; Goldsmith, C. S.; Zaki, S. R.; Peret, T.; Emery, S.; Tong, S.; Urbani, C.; Comer, J. A.; Lim, W. et al. A novel coronavirus associated with severe acute respiratory syndrome. *N. Engl. J. Med.* **2003**, *348*, 1953–1966.

(4) Marra, M. A.; Jones, S. J. M.; Astell, C. R.; Holt, R. A.; Brooks-Wilson, A.; Butterfield, Y. S. N.; Khattra, J.; Asano, J. K.; Barber, S. A.; Chan, S. Y. et al. The Genome sequence of the SARS-associated coronavirus. *Science* **2003**, *300*, 1399–1404.

(5) Rota, P. A.; Oberste, M. S.; Monroe, S. S.; Nix, W. A.; Campagnoli, R.; Icenogle, J. P.; Peñaranda, S.; Bankamp, B.; Maher, K.; Chen, M.-H. et al. Characterization of a novel coronavirus associated with severe acute respiratory syndrome. *Science* **2003**, *300*, 1394–1399.

(6) van der Hoek, L.; Pyrc, K.; Jebbink, M. F.; Vermeulen-Oost, W.; Berkhout, R. J. M.; Wolthers, K. C.; Wertheim-van Dillen, P. M. E.; Kaandorp, J.; Spaargaren, J.; Berkhout, B. Identification of a new human coronavirus. *Nat. Med.* **2004**, *10*, 368–373.

(7) Woo, P. C. Y.; Lau, S. K. P.; Chu, C.-m.; Chan, K.-h.; Tsoi, H.-w.; Huang, Y.; Wong, B. H. L. et al.; Poon, R. W. S.; Cai, J. J.; Luk, W.-k. et al. Characterization and complete genome sequence of a novel coronavirus, coronavirus HKU1, from patients with pneumonia. *J. Virol.* **2005**, *79*, 884–895.

(8) de Groot, R. J.; Baker, S. C.; Baric, R. S.; Brown, C. S.; Drosten, C.; Enjuanes, L.; Fouchier, R. A. M.; Galiano, M.; Gorbalenya, A. E.; Memish, Z. A. et al. Middle East respiratory syndrome coronavirus (MERS-CoV): announcement of the Coronavirus Study Group. *J. Virol.* **2013**, *87*, 7790–7792.

(9) Wu, Q.; Zhang, Y.; Lü, H.; Wang, J.; He, X.; Liu, Y.; Ye, C.; Lin, W.; Hu, J.; Ji, J. et al. The E protein is a multifunctional membrane protein of SARS-CoV. *Genomics Proteomics Bioinformatics* **2003**, *1*, 131–144.

(10) Shen, X.; Xue, J.-H.; Yu, C.-Y.; Luo, H.-B.; Qin, L.; Yu, X.-J.; Chen, J.; Chen, L.-L.; Xiong, B.; Yue, L.-D. et al. Small envelope protein E of SARS: cloning, expression, pu-

rification, CD determination, and bioinformatics analysis. *Acta Pharmacol. Sin.* **2003**, *24*, 505–511.

(11) Nal, B.; Chan, C.; Kien, F.; Siu, L.; Tse, J.; Chu, K.; Kam, J.; Staropoli, I.; Crescenzo-Chaigne, B.; Escriou, N. et al. Differential maturation and subcellular localization of severe acute respiratory syndrome coronavirus surface proteins S, M and E. *J. Gen. Virol.* **2005**, *86*, 1423–1434.

(12) Lopez, L. A.; Riffle, A. J.; Pike, S. L.; Gardner, D.; Hogue, B. G. Importance of conserved cysteine residues in the coronavirus envelope protein. *J. Virol.* **2008**, *82*, 3000–3010.

(13) Arbely, E.; Khattari, Z.; Brotons, G.; Akkawi, M.; Salditt, T.; Arkin, I. T. A highly unusual palindromic transmembrane helical hairpin formed by SARS coronavirus E protein. *J. Mol. Biol.* **2004**, *341*, 769–779.

(14) Torres, J.; Parthasarathy, K.; Lin, X.; Saravanan, R.; Kukol, A.; Liu, D. X. Model of a putative pore: the pentameric alpha-helical bundle of SARS coronavirus E protein in lipid bilayers. *Biophys. J.* **2006**, *91*, 938–947.

(15) Cohen, J. R.; Lin, L. D.; Machamer, C. E. Identification of a Golgi complex-targeting signal in the cytoplasmic tail of the severe acute respiratory syndrome coronavirus envelope protein. *J. Virol.* **2011**, *85*, 5794–5803.

(16) Teoh, K.-T.; Siu, Y.-L.; Chan, W.-L.; Schlüter, M. A.; Liu, C.-J.; Peiris, J. S. M.; Bruzzone, R.; Margolis, B.; Nal, B. The SARS coronavirus E protein interacts with PALS1 and alters tight junction formation and epithelial morphogenesis. *Mol. Biol. Cell.* **2010**, *21*, 3838–3852.

(17) Yang, Y.; Xiong, Z.; Zhang, S.; Yan, Y.; Nguyen, J.; Ng, B.; Lu, H.; Brendese, J.; Yang, F.; Wang, H. et al. Bcl-xL inhibits T-cell apoptosis induced by expression of SARS coronavirus E protein in the absence of growth factors. *Biochem. J.* **2005**, *392*, 135–143.

(18) DeDiego, M. L.; Nieto-Torres, J. L.; Jiménez-Guardeño, J. M.; Regla-Nava, J. A.; Alvarez, E.; Oliveros, J. C.; Zhao, J.; Fett, C.; Perlman, S.; Enjuanes, L. Severe acute respiratory syndrome coronavirus envelope protein regulates cell stress response and apoptosis. *PLoS Pathog.* **2011**, *7*, e1002315.

(19) Pervushin, K.; Tan, E.; Parthasarathy, K.; Lin, X.; Jiang, F. L.; Yu, D.; Vararattanavech, A.; Soong, T. W.; Liu, D. X.; Torres, J. Structure and inhibition of the SARS coronavirus envelope protein ion channel. *PLoS Pathog.* **2009**, *5*, e1000511.

(20) Torres, J.; Maheswari, U.; Parthasarathy, K.; Ng, L.; Liu, D. X.; Gong, X. Conductance and amantadine binding of a pore formed by a lysine-flanked transmembrane domain of SARS coronavirus envelope protein. *Protein. Sci.* **2007**, *16*, 2065–2071.

(21) Verdiá-Báguena, C.; Nieto-Torres, J. L.; Alcaraz, A.; Dediego, M. L.; Enjuanes, L.; Aguilella, V. M. Analysis of SARS-CoV E protein ion channel activity by tuning the protein and lipid charge. *Biochim. Biophys. Acta* **2013**, *1828*, 2026–2031.

(22) Liao, Y.; Yuan, Q.; Torres, J.; Tam, J. P.; Liu, D. X. Biochemical and functional characterization of the membrane association and membrane permeabilizing activity of the severe acute respiratory syndrome coronavirus envelope protein. *Virology* **2006**, *349*, 264–275.

(23) Liao, Y.; Lescar, J.; Tam, J. P.; Liu, D. X. Expression of SARS-coronavirus envelope protein in Escherichia coli cells alters membrane permeability. *Biochem. Biophys. Res. Commun.* **2004**, *325*, 374–380.

(24) Wilson, L.; Gage, P.; Ewart, G. Hexamethylene amiloride blocks E protein ion channels and inhibits coronavirus replication. *Virology* **2006**, *353*, 294–306.

(25) Wilson, L.; McKinlay, C.; Gage, P.; Ewart, G. SARS coronavirus E protein forms cation-selective ion channels. *Virology* **2004**, *330*, 322–331.

(26) Nieto-Torres, J. L.; Dediego, M. L.; Alvarez, E.; Jiménez-Guardeño, J. M.; Regla-Nava, J. A.; Llorente, M.; Kremer, L.; Shuo, S.; Enjuanes, L. Subcellular location and topology of severe acute respiratory syndrome coronavirus envelope protein. *Virology* **2011**, *415*, 69–82.

(27) Bos, E. C.; Luytjes, W.; van der Meulen, H. V.; Koerten, H. K.; Spaan, W. J. The production of recombinant infectious DI-particles of a murine coronavirus in the absence of helper virus. *Virology* **1996**, *218*, 52–60.

(28) Vennema, H.; Godeke, G. J.; Rossen, J. W.; Voorhout, W. F.; Horzinek, M. C.; Opstelten, D. J.; Rottier, P. J. Nucleocapsid-independent assembly of coronavirus-like particles by co-expression of viral envelope protein genes. *EMBO. J.* **1996**, *15*, 2020–2028.

(29) Siu, Y. L.; Teoh, K. T.; Lo, J.; Chan, C. M.; Kien, F.; Escriou, N.; Tsao, S. W.; Nicholls, J. M.; Altmeyer, R.; Peiris, J. S. M. et al. The M, E, and N structural proteins of the severe acute respiratory syndrome coronavirus are required for efficient assembly, trafficking, and release of virus-like particles. *J. Virol.* **2008**, *82*, 11318–11330.

(30) Ruch, T. R.; Machamer, C. E. The hydrophobic domain of infectious bronchitis virus E protein alters the host secretory pathway and is important for release of infectious virus. *J. Virol.* **2011**, *85*, 675–685.

(31) Ji, H.-L.; Song, W.; Gao, Z.; Su, X.-F.; Nie, H.-G.; Jiang, Y.; Peng, J.-B.; He, Y.-X.; Liao, Y.; Zhou, Y.-J. et al. SARS-CoV proteins decrease levels and activity of human ENaC via activation of distinct PKC isoforms. *Am. J. Physiol. Lung Cell. Mol. Physiol.* **2009**, *296*, L372–383.

(32) Maeda, J.; Maeda, A.; Makino, S. Release of coronavirus E protein in membrane vesicles from virus-infected cells and E protein-expressing cells. *Virology* **1999**, *263*, 265–272.

(33) Kuo, L.; Masters, P. S. The small envelope protein E is not essential for murine coronavirus replication. *J. Virol.* **2003**, *77*, 4597–4608.

(34) Dediego, M. L.; Pewe, L.; Alvarez, E.; Rejas, M. T.; Perlman, S.; Enjuanes, L. Pathogenicity of severe acute respiratory coronavirus deletion mutants in hACE-2 transgenic mice. *Virology* **2008**, *376*, 379–389.

(35) DeDiego, M. L.; Alvarez, E.; Almazán, F.; Rejas, M. T.; Lamirande, E.; Roberts, A.; Shieh, W.-J.; Zaki, S. R.; Subbarao, K.; Enjuanes, L. A severe acute respiratory syndrome coronavirus that lacks the E gene is attenuated in vitro and in vivo. *J. Virol.* **2007**, *81*, 1701–1713.

(36) Raamsman, M. J.; Locker, J. K.; de Hooge, A.; de Vries, A. A.; Griffiths, G.; Vennema, H.; Rottier, P. J. Characterization of the coronavirus mouse hepatitis virus strain A59 small membrane protein E. *J. Virol.* **2000**, *74*, 2333–2342.

(37) Alvarez, E.; DeDiego, M. L.; Nieto-Torres, J. L.; Jiménez-Guardeño, J. M.; Marcos-Villar, L.; Enjuanes, L. The envelope protein of severe acute respiratory syndrome coronavirus interacts with the non-structural protein 3 and is ubiquitinated. *Virology* **2010**, *402*, 281–291.

(38) Keng, C.-T.; Akerström, S.; Leung, C. S.-W.; Poon, L. L. M.; Peiris, J. S. M.; Mirazimi, A.; Tan, Y.-J. SARS coronavirus 8b reduces viral replication by down-regulating E via an ubiquitin-independent proteasome pathway. *Microbes. Infect.* **2011**, *13*, 179–188.

(39) Keng, C.-T.; Choi, Y.-W.; Welkers, M. R. A.; Chan, D. Z. L.; Shen, S.; Gee Lim, S.; Hong, W.; Tan, Y.-J. The human severe acute respiratory syndrome coronavirus (SARS-CoV) 8b protein is distinct from its counterpart in animal SARS-CoV and down-regulates the expression of the envelope protein in infected cells. *Virology* **2006**, *354*, 132–142.

(40) Fett, C.; DeDiego, M. L.; Regla-Nava, J. A.; Enjuanes, L.; Perlman, S. Complete protection against severe acute respiratory syndrome coronavirus-mediated lethal respiratory disease in aged mice by immunization with a mouse-adapted virus lacking E protein. *J. Virol.* **2013**, *87*, 6551–6559.

(41) Peng, H.; Yang, L.-t.; Li, J.; Lu, Z.-q.; Wang, L.-y.; Koup, R. A.; Bailer, R. T.; Wu, C.-y. Human memory T cell responses to SARS-CoV E protein. *Microbes. Infect.* **2006**, *8*, 2424–2431.

(42) Zhang, X.; Wu, K.; Yue, X.; Zhu, Y.; Wu, J. Inhibition of SARS-CoV gene expression by adenovirus-delivered small hairpin RNA. *Intervirology* **2007**, *50*, 63–70.

(43) Meng, B.; Lui, Y.-w.; Meng, S.; Cao, C.; Hu, Y. Identification of effective siRNA blocking the expression of SARS viral envelope E and RDRP genes. *Mol. Biotechnol.* **2006**, *33*, 141–148.

(44) Netland, J.; DeDiego, M. L.; Zhao, J.; Fett, C.; Alvarez, E.; Nieto-Torres, J. L.; Enjuanes, L.; Perlman, S. Immunization with an attenuated severe acute respiratory syndrome coronavirus deleted in E protein protects against lethal respiratory disease. *Virology* **2010**, *399*, 120–128.

(45) Lamirande, E. W.; DeDiego, M. L.; Roberts, A.; Jackson, J. P.; Alvarez, E.; Sheahan, T.; Shieh, W.-J.; Zaki, S. R.; Baric, R.; Enjuanes, L.; Subbarao, K. A live attenuated severe acute respiratory syndrome coronavirus is immunogenic and efficacious in golden Syrian hamsters. *J. Virol.* **2008**, *82*, 7721–7724.

(46) Yuan, Q.; Liao, Y.; Torres, J.; Tam, J. P.; Liu, D. X. Biochemical evidence for the presence of mixed membrane topologies of the severe acute respiratory syndrome coronavirus envelope protein expressed in mammalian cells. *FEBS. Lett.* **2006**, *580*, 3192–3200.

(47) Maeda, J.; Repass, J. F.; Maeda, A.; Makino, S. Membrane topology of coronavirus E protein. *Virology* **2001**, *281*, 163–169.

(48) Khattari, Z.; Brotons, G.; Akkawi, M.; Arbely, E.; Arkin, I. T.; Salditt, T. SARS coronavirus E protein in phospholipid bilayers: an x-ray study. *Biophys. J.* **2006**, *90*, 2038–2050.

(49) Arkin, I. T.; Brunger, A. T. Statistical analysis of predicted transmembrane alpha-helices. *Biochim. Biophys. Acta* **1998**, *1429*, 113–128.

(50) Parthasarathy, K.; Ng, L.; Lin, X.; Liu, D. X.; Pervushin, K.; Gong, X.; Torres, J. Structural flexibility of the pentameric SARS coronavirus envelope protein ion channel. *Biophys. J.* **2008**, *95*, L39–41.

(51) Torres, J.; Kukol, A.; Goodman, J. M.; Arkin, I. T. Site-specific examination of secondary structure and orientation determination in membrane proteins: the peptidic (13)C=(18)O group as a novel infrared probe. *Biopolymers* **2001**, *59*, 396–401.

(52) Manor, J.; Feldblum, E. S.; Zanni, M. T.; Arkin, I. T. Environment Polarity in Proteins Mapped Noninvasively by FTIR Spectroscopy. *J. Phys. Chem. Lett.* **2012**, *3*, 939–944.

(53) Manor, J.; Arkin, I. T. Gaining insight into membrane protein structure using isotope-edited FTIR. *Biochim. Biophys. Acta* **2012**, *1828*, 2256–2264.

(54) Harrick, N. J. *Internal reflection spectroscopy*; Interscience Publishers: New York, 1967.

(55) Manor, J.; Khattari, Z.; Salditt, T.; Arkin, I. T. Disorder influence on linear dichroism analyses of smectic phases. *Biophys. J.* **2005**, *89*, 563–571.

(56) Axelsen, P. H.; Citra, M. J. Orientational order determination by internal reflection infrared spectroscopy. *Prog. Biophys. Mol. Biol.* **1996**, *66*, 227–253.

(57) Manor, J.; Mukherjee, P.; Lin, Y.-S.; Leonov, H.; Skinner, J. L.; Zanni, M. T.; Arkin, I. T. Gating mechanism of the influenza A M2 channel revealed by 1D and 2D IR spectroscopies. *Structure* **2009**, *17*, 247–254.

(58) Brünger, A. T.; Adams, P. D.; Clore, G. M.; DeLano, W. L.; Gros, P.; Grosse-Kunstleve, R. W.; Jiang, J. S.; Kuszewski, J.; Nilges, M.; Pannu, N. S. et al. Crystallography & NMR system: A new software suite for macromolecular structure determination. *Acta Crystallogr. D Biol. Crystallogr.* **1998**, *54*, 905–921.

(59) Brünger, A. T. Version 1.2 of the Crystallography and NMR system. *Nat. Protoc.* **2007**, *2*, 2728–2733.

(60) Jorgensen, W. L.; Tirado-Rives, J. The OPLS [optimized potentials for liquid simulations] potential functions for proteins, energy minimizations for crystals of cyclic peptides and crambin. *J. Am. Chem. Soc.* **1988**, *110*, 1657–1666.